2016

Seismic retrofit of industrial silos by means of base isolation devices

Kanyilmaz, Alper

ECCOMAS Congress 2016
VII European Congress on Computational Methods in Applied Sciences and Engineering
M. Papadrakakis, V. Papadopoulos, G. Stefanou, V. Plevris (eds.)
Crete Island, Greece, 5–10 June 2016

SEISMIC RETROFIT OF INDUSTRIAL SILOS BY MEANS OF BASE ISOLATION DEVICES

Alper Kanyilmaz[1], Carlo Andrea Castiglioni[1], and Julia Georgi[1]

[1]Neapolis University in Cyprus

School of Architecture, Land & Environmental Sciences

Zdanaes Ave. Paphos 8042-Cyprus

alperkanyilmaz@gmail.com, c.castiglioni@nup.ac.cy, j.georgi@nup.ac.cy

Keywords: Silos, seismic retrofit, seismic isolation, curved surface sliders

Abstract. *Silos are industrial facilities used for storing a huge range of different materials. In the last decades, many silos were damaged by natural events, among which the seismic events are the most significant. Indeed many plants are located in territories in which seismic risk is not negligible. Furthermore, most of these plants have been designed, and built before the latest updates of the seismic design codes took place, and most of them are prone to earth-quakes. In this study, seismic behaviour of an existing industrial steel silo system in Italy has been investigated, and a retrofit solution has been proposed making use of seismic isolation technology. Incremental dynamic analysis method has been used in order to evaluate the seismic performance of both the non-isolated and isolated cases. Structural and economic benefits of the seismic isolation retrofitting solution has been quantified, and comparisons are shown. The study has been realized thanks to EU-RFCS research fund for PROINDUSTRY project [1].*

1 SILOS CASE STUDY

The case study is composed of three silos, elevated on a steel structure, constructed next to another 2 elevated silos. It's a silo system from SOLVAY Italy (Figure 1).

Figure 1 Case study

Main characteristics of the system are the following:

Internal radius of silos:	1.75 m
Total height of silos:	13.356 m
Thickness of silo body:	Changes along height from 12 to 8 mm.
Steel:	Fe360b
Silo content:	Sodium percarbonate
E =	210000 MPa
ν =	0,3
ϒsteel =	7850 kg/m3
ϒcontent =	1200 kg/m3 (sodium percarbonate)

Layout of the system can be seen in Figure 2. The stairs and connection structure between three silos are neglected for simplicity, since the rigidity and the mass of the silos probably will lead the global behaviour, without an important effect of the connecting structures and stairs.

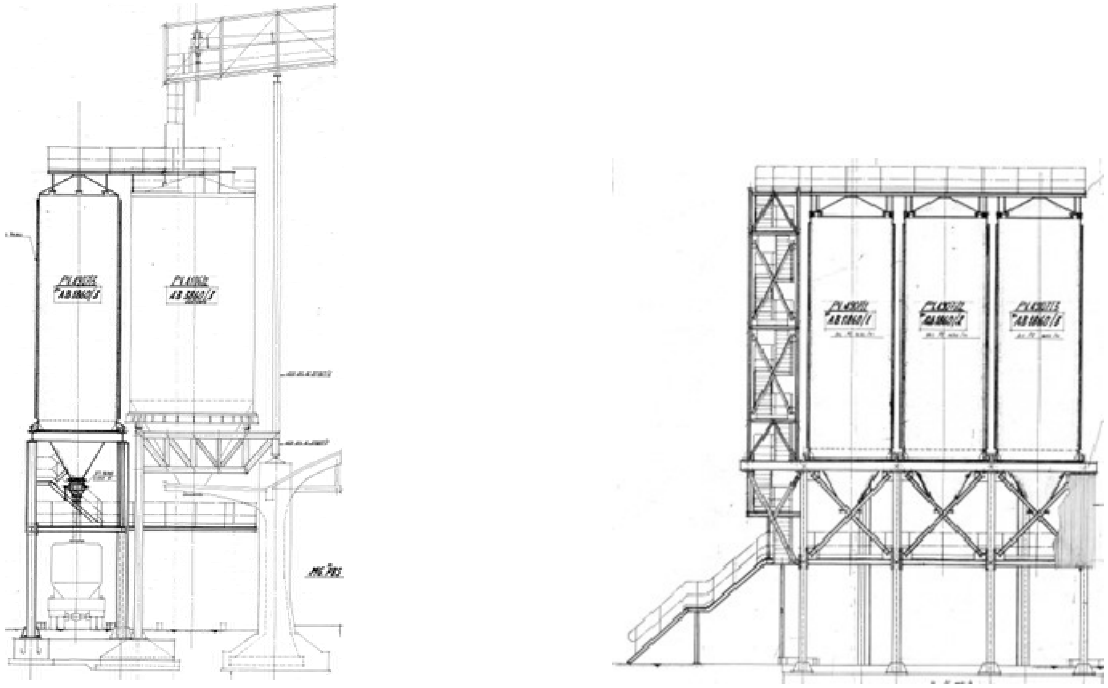

a. Transversal view b. Longitudinal view

Figure 2 System layout

The silos are connected to the support structure by means of stiffener plates (Figure 3). 24 stiffener plates are welded to the silo wall, equally spaced around its perimeter. These stiffener plates are then welded to the ring beam with 150x30 mm cross section. The ring beam is bolted to the support structure beams.

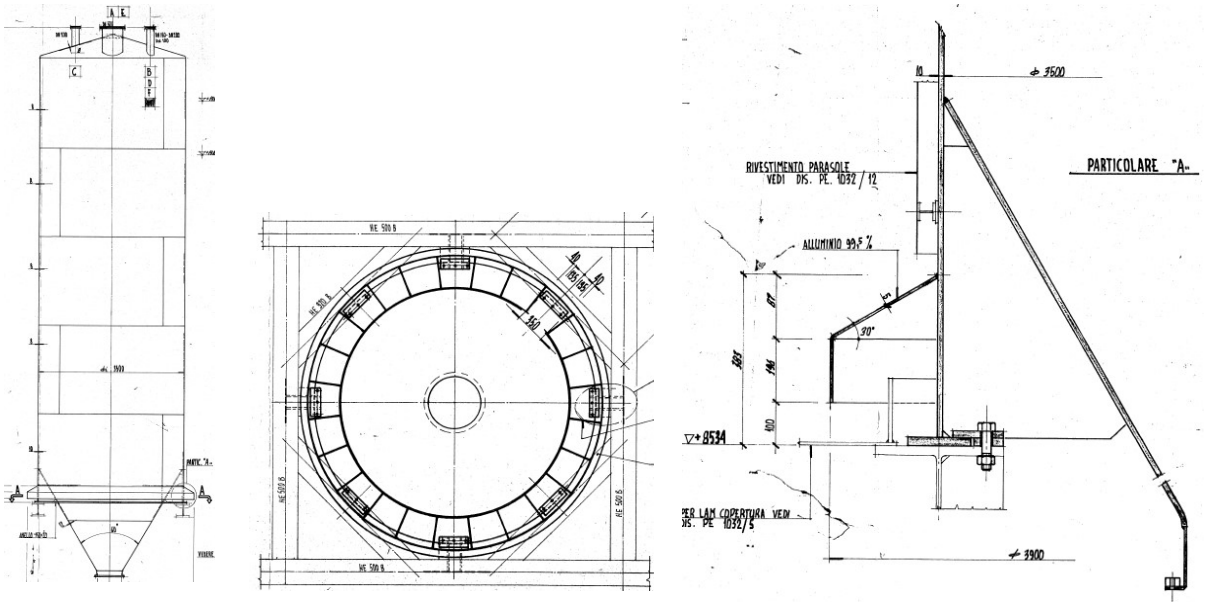

Figure 3 Ring beam-silo connection detail

Three main levels are considered in the numerical model:

Level +0 mm: The columns are fixed at this level, which corresponds to "-650.00 mm" level of the drawings (Figure 4.a)

Level +4850 mm: First beam level (Figure 4.c)

Level +8934 mm: Second beam level (Figure 4.d)

Level +20580 mm: Top point of silos (Figure 4.b)

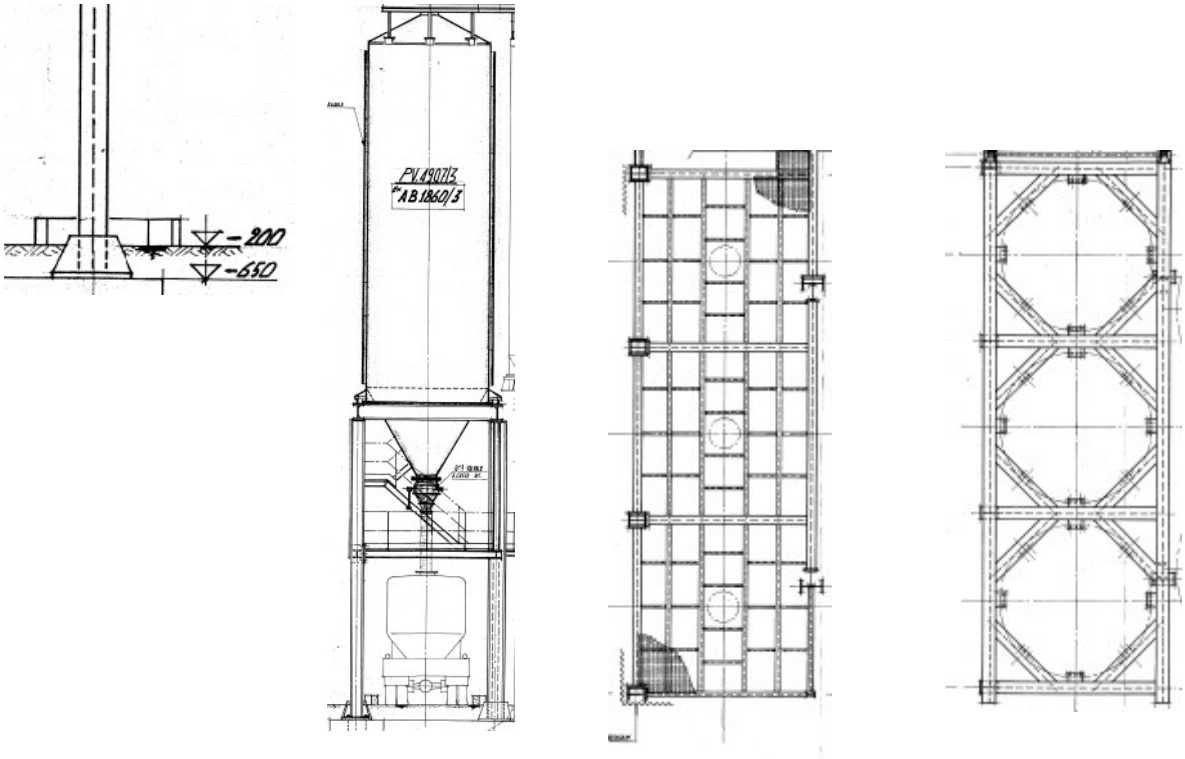

a. Ground level b. Section view c. +4850 mm plan view d. +8934 mm plan view

Figure 4 Different levels of the system

The supporting structure is an asymmetric steel frame braced only in longitudinal direction, with different bracing layouts in two sides (Figure 5).

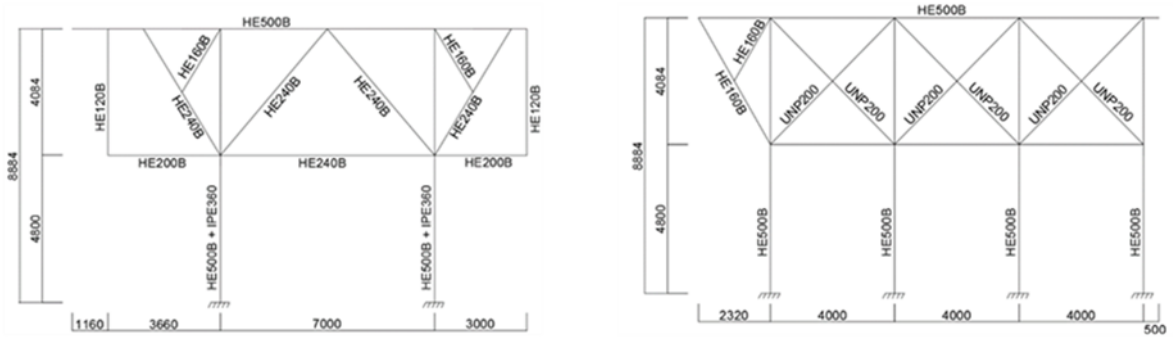

a. V-braced side b. X-braced side

Figure 5 Two sides of the structure

2 NUMERICAL MODEL

Numerical model is composed of silo bodies made of shell elements, steel structure made of beam elements formulated by fiber-based distributed plasticity approach [2], steel plate elements and rigid links that connect silo bodies and steel structure. Bracing elements are given initial imperfections according to EC3, as shown in Table 1.

S235 Steel	e_0 [mm]
HE240B [m]	35,9
HE160B [m]	15,9
HE240B [m]	16,0
UPN200 [m]	19,1

Table 1 Initial imperfections for bracing elements

The supporting structure has different bracing configurations in two sides of the frame (Figure 6.a.b). Lumped dynamic masses simulate the silo content, distributed at 7 levels inside silo, connected to silo walls by rigid links (Figure 6.c).

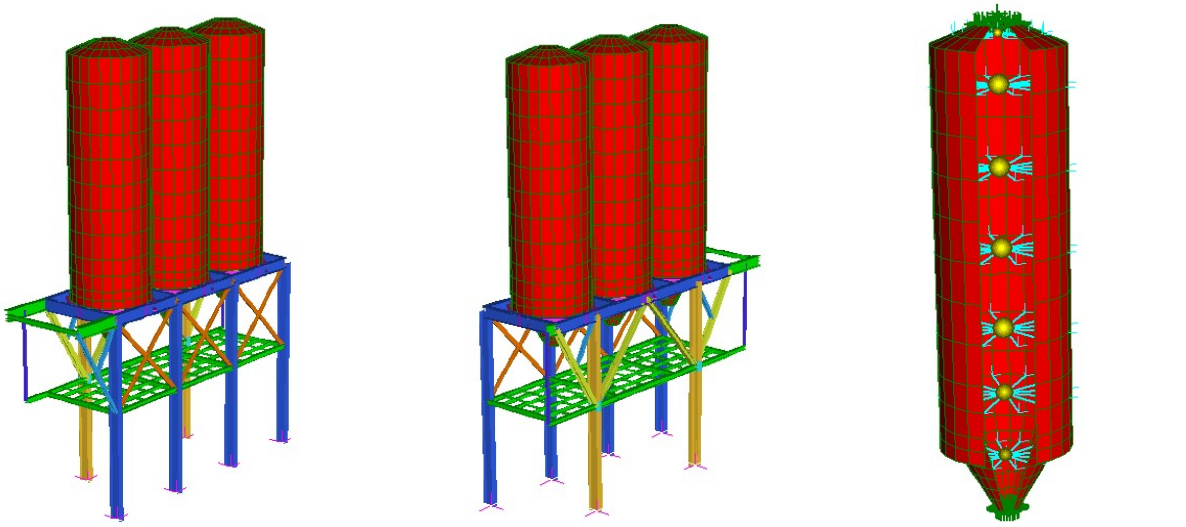

a. Model view 1 (X-braced side) b. Model view 2 (V-braced side) c. Lumped masses

Figure 6 Numerical model

The connection between HE500B longitudinal beams and silo are simulated with rigid links in the model. The connection between silo and ring beam is composed of 24 steel plates, which are simulated with shell elements in the model.

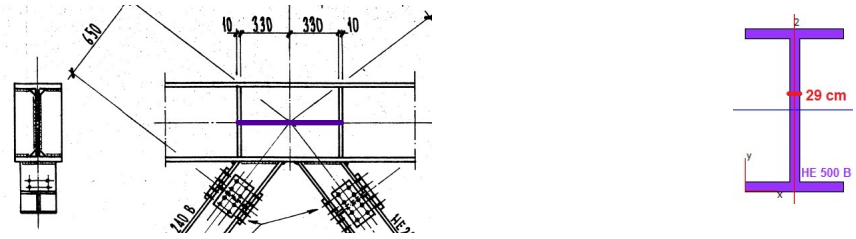

Figure 7 Reinforcement of the joints

As shown in Figure 7, the reinforcements of nodes are simulated by an ideal section with a doubled thickness of the core between the two reinforcement plates: stiffening the joint in this way, its behaviour is almost the same that the real one with the stiffening due only to the two reinforcement plates. The main areas where the joints are stiffened are contact points between the silos and the frame, and the joint between the two composite columns HE500B+IPE360 and the beams at the first floor.

Total mass of the system is 453,9 tons with following components:

Silo content: 391,1 tons

Silo body steel weight: 31,37 tons

Structural steel: 31,43 tons

Stress-strain relationship of the steel material has been defined with the following parameters:

Yield strength fy = 235 MPa
Ultimate strength fu = 360 MPa
Kinematic strain hardening: 1 %
Ultimate strain = 0.06

In Table 2 Modal analysis results, modal analysis results are reported. Mode shapes are shown in Figure 8 Mode shapes.

	Period	Mass participation
1st global mode in y direction (transversal)	1.2 sec	97.96%
2nd global mode in x direction (longitudinal)	1.05 sec	90.177%
3rd global mode in z direction (vertical)	0.13 sec	95.541%
1st global torsional mode	0.84 sec	9.4%

Table 2 Modal analysis results

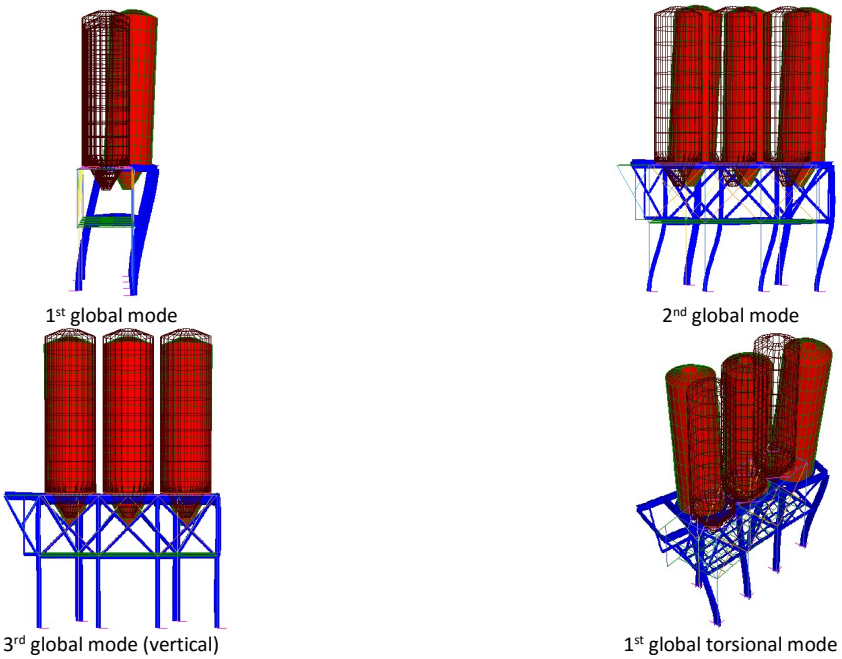

Figure 8 Mode shapes

3 FAILURE MECHANISMS OBSERVED IN THE ORIGINAL STRUCTURE

Results of Incremental Dynamic Analysis performed on the original structure have been presented in deliverable 2.3. In this report, only failure mechanisms of the original structure are presented, in order to provide the degree of improvement by means of seismic isolation devices.

In the original structure, yield takes places at column bases even in the analysis with low scale factors. Increasing the intensity, the plastic behaviour is redistributed to the column ends, bracings, and connections between silo and supporting structure (Figure 9).

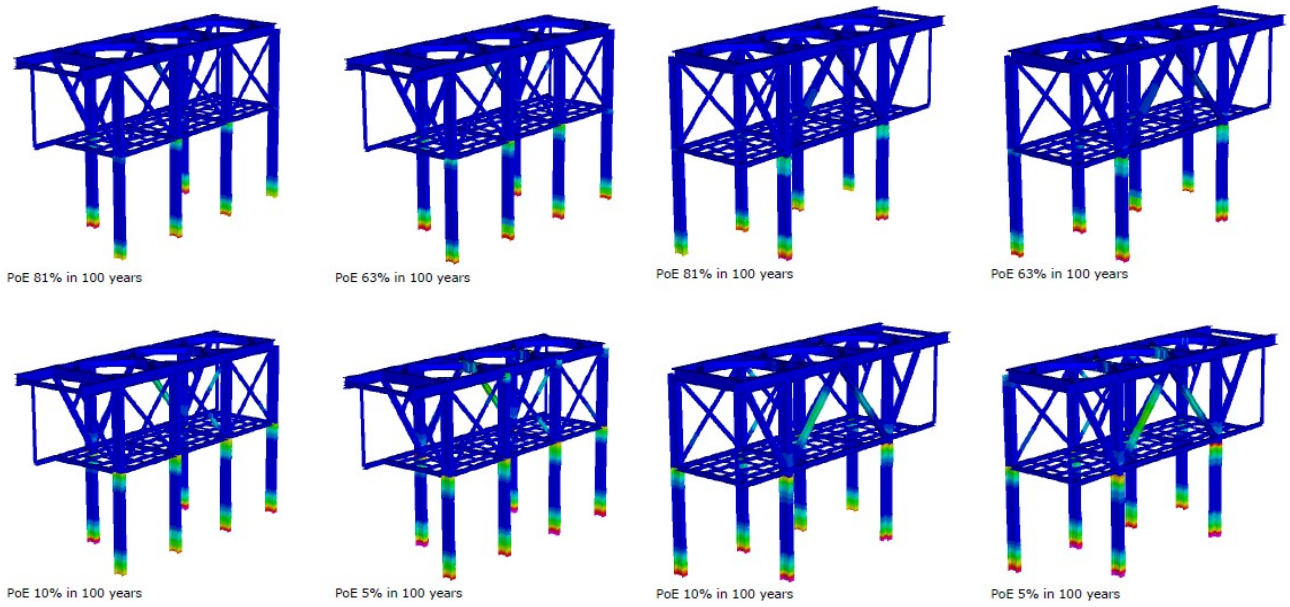

a. X-braced side b. V-braced side

Figure 9 Failure mechanisms of the original structure

Figure 10 shows that the numerically obtained failure mechanisms represent common structural damages that can be observed after strong earthquakes, such as Van Earthquake. Therefore, the seismic retrofitting solution should address these criticalities.

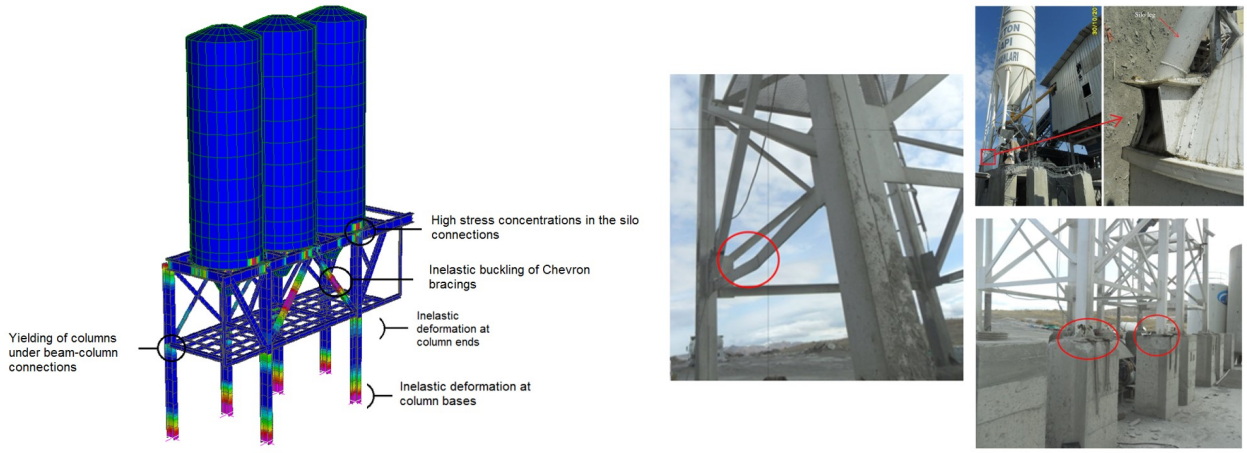

a. Failure mechanisms obtained from numerical analysis b. Damages observed on the support structure of elevated silos after Van Earthquake (2011)

Figure 10 Structural damages observed in Van Earthquake and numerically obtained failure mechanisms [3]

4 DESIGN OF SEISMIC ISOLATION SOLUTION

To retrofit the structure, a single sliding pendulum isolator has been designed in cooperation with project partner MAURER [4]. A static diagram of the forces acting in a sliding pendulum isolator used for the retrofitting is shown in Figure 11, while the force - displacement relationship is displayed in Figure 12.

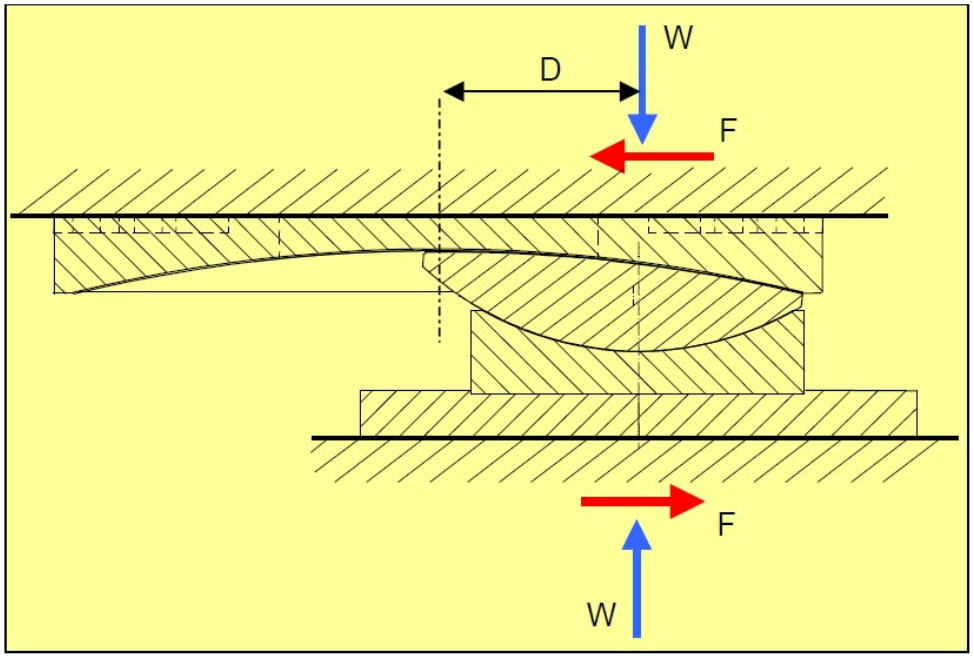

Figure 11 Forces acting in a sliding pendulum isolator

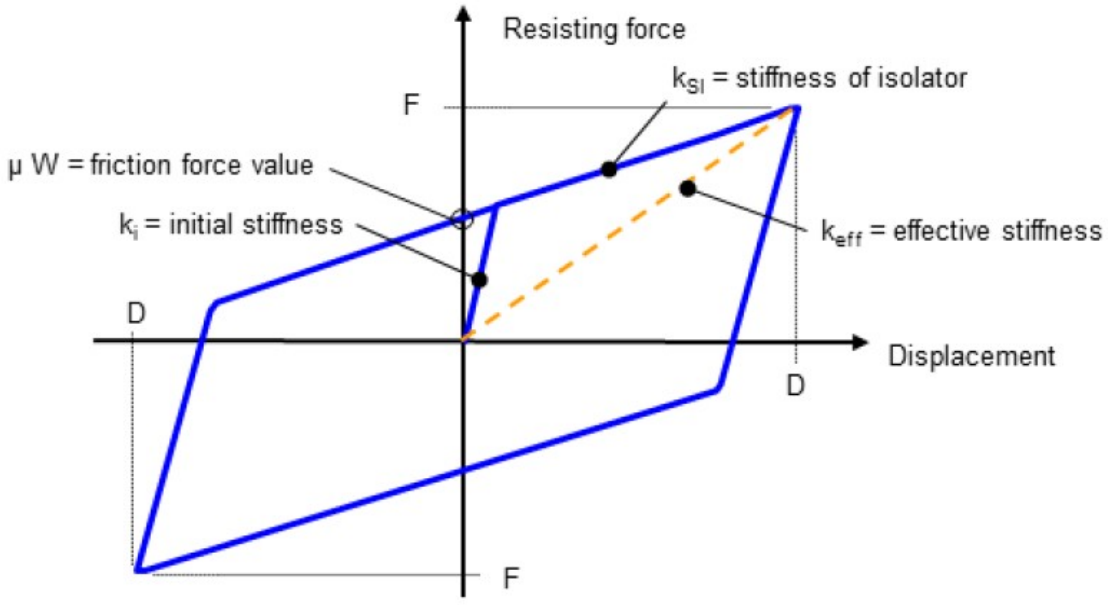

Figure 12 Force - displacement relationship in a sliding pendulum isolator

The equations governing the behaviour of a single isolators are the following:

Response period of the Isolator $$T = 2 \cdot \pi \cdot \sqrt{\frac{R}{g}} \cong 2 \cdot \sqrt{R}$$

Horizontal resisting force $$F = \frac{W}{R} \cdot d + \mu \cdot W \cdot sgn(d)$$

Horizontal stiffness due to the vertical load $$K_H = \frac{W}{R}$$

Effective stiffness $$K_{eff} = \frac{W}{R} + \frac{\mu \cdot W}{D}$$

Effective response period $$T_{eff} = 2 \cdot \pi \cdot \sqrt{\frac{R}{K_{eff} \cdot g}}$$

Damping due to friction $$\beta_{eff} = \frac{2}{\pi} \cdot \frac{\mu}{\frac{D}{R} + \mu}$$

Vertical displacement $$\delta_V \cong \frac{1}{2} \frac{D}{R^2}$$

Re-centering criterion $$\frac{D}{R} > \mu$$

Where W is the vertical load acting on the isolator agent, μ is the dynamic friction factor, d is the horizontal displacement, D is the horizontal speed and R is the radius of curvature. Note that the horizontal stiffness is linked to the load acting on the isolators: in an optimal design should therefore a different isolator should be adopted for each design vertical load.

In particular an isolator can be modelled by placing in parallel the two following elements, as shown in Figure 13.

1) Point Contact element: by means of an element of this type it is possible to define the friction factor and the vertical stiffness of the isolator. You can also define the yield surface of the isolator (rectangular or elliptical) and the friction model (elastic or plastic). Using an elliptical surface we ensure that the point at which the isolator begins to flow is the same in all directions, while the plastic friction model governs the hysteretic behaviour of the isolator.

2) Connection element: using an element of this type the stiffness of the isolator to sliding in horizontal directions can be defined.

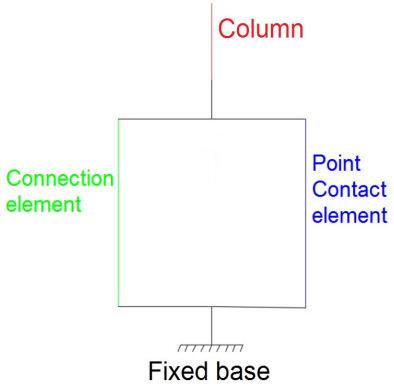

Figure 13 Modelling of the isolator in Straus7

It should be noticed that in Strand7 the length of the two elements of the isolator is not influencing the isolator behaviour, which is completely defined by the intrinsic properties of the

two elements. Assuming a fictitious length of the isolators equal to 500 mm, to each column of the previously modelled structure are added a Point Contact and a Connection element. The modelled isolators are shown by Strand7 as lines, whose lower point is stuck to the ground and whose upper end is connected to the column, as shown in Figure 14.

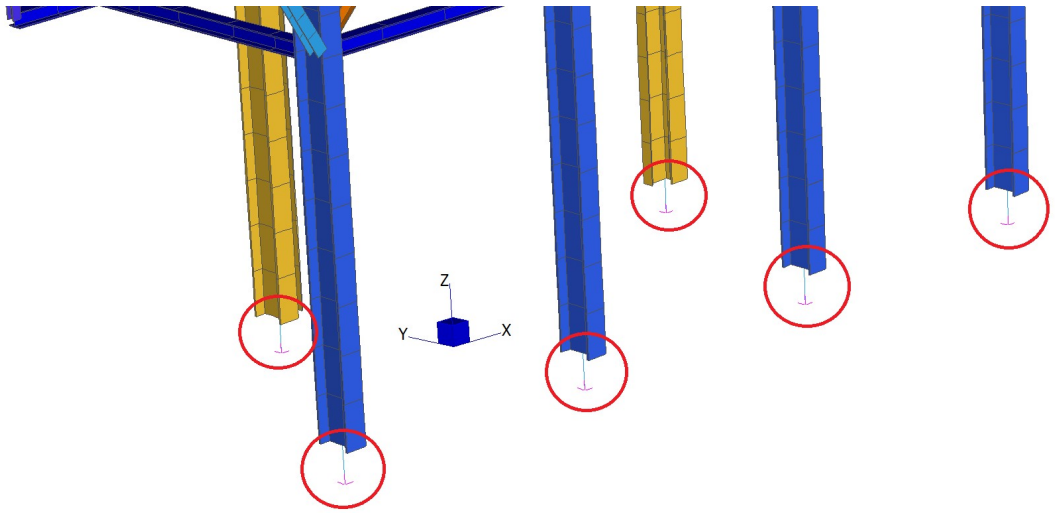

Figure 14 modelling the isolators in Straus7

To verify the correctness of the isolation system modelling, a non-linear static analysis was carried out, gradually applying a hypothetical design displacement of ± 300mm to the isolators as shown in Figure 15. A period of 4 seconds hence a sliding stiffness k_s equal to 0.187 kN / mm) and 4 % friction factor was assumed for all the isolators.

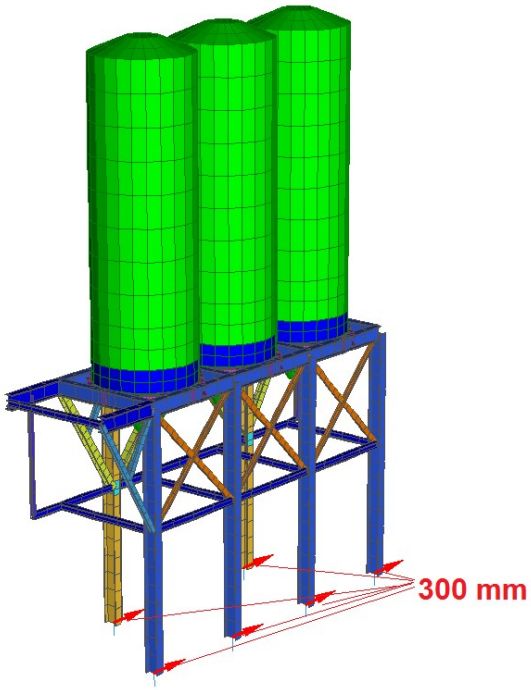

Figure 15 Displacements imposed to the isolators

With reference to the nodes numbering shown in Figure 3.50, let's consider, for example, the isolator in the node 5, on which acts a vertical load of 777.8 kN. The force-displacement response of the isolator in the node 5, obtained by the nonlinear static analysis is shown in Figure 16, where the displacements are dimensionless for a better understanding.

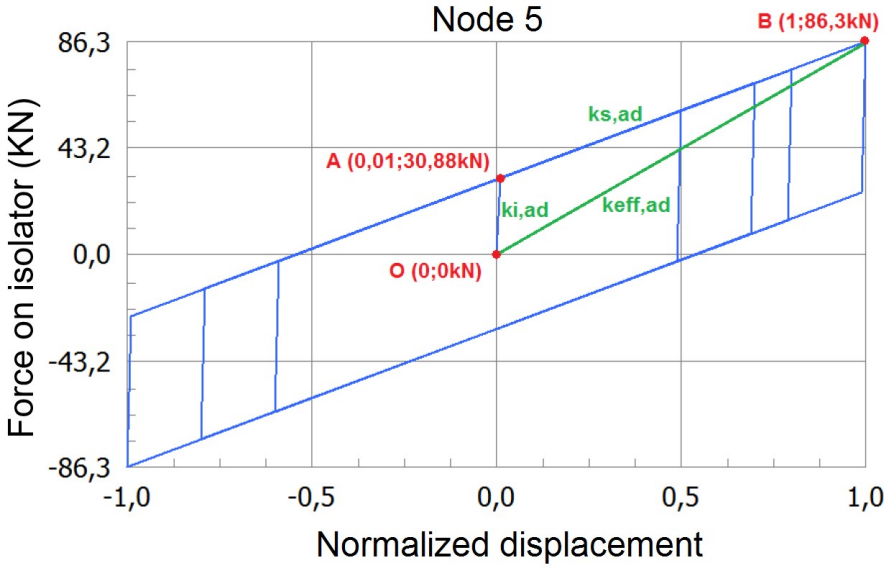

Figure 16 Constitutive law of the isolator in node 5 in terms force-displacement (period 4 seconds and friction factor 4%)

From the constitutive law obtained by the nonlinear static analysis, the initial stiffness k_i and the sliding stiffness k_s of the isolator are:

$$k_{i,ad} = \frac{y_A - y_O}{x_A - y_O} = \frac{30{,}88\ kN}{0{,}01} = 3088\ kN$$

$$k_{s,ad} = \frac{y_B - y_A}{x_B - y_A} = \frac{86{,}3\ kN - 30{,}88 kN}{1 - 0{,}01} = \frac{55{,}42\ kN}{0{,}99} = 55{,}98\ kN$$

As the constitutive law of the isolator has been plotted by normalizing the displacements, the stiffness must also be calculated scaled to the hypothetical design displacement for the isolators, assumed equal to 300 mm:

$$k_i = \frac{k_{i,ad}}{300\ mm} = \frac{3088\ kN}{300\ mm} = 10{,}293\ \frac{kN}{mm}$$

$$k_s = \frac{k_{s,ad}}{300\ mm} = \frac{55{,}98\ kN}{300\ mm} = 0{,}187\ \frac{kN}{mm}$$

It can be noticed that the sliding stiffness ks coincides with that initially assumed, that is:

$$k_{i,def} = \frac{\mu W}{D_y \cdot 300\ mm} = \frac{0{,}04 \cdot 777{,}8\ kN}{0{,}01 \cdot 300\ mm} = 10{,}37\ \frac{kN}{mm}$$

Where μ is the friction factor, D_y is conventionally assumed as 0.01 and W is the load applied on the isolator. It is observed that also in this case $k_{i,def}$, obtained by means of the theoretical definition , is approximated to k_i obtained from the actual constitutive law of the isolator. Finally, the effective stiffness related to the dimensionless displacement $K_{eff,ad}$ and to the design displacement K_{eff} are:

$$k_{eff,ad} = \frac{y_B - y_O}{x_B - y_O} = 86{,}3\ kN$$

$$k_{eff} = \frac{k_{eff,ad}}{300\ mm} = 0{,}288\ \frac{kN}{mm}$$

With reference to the definition of effective stiffness, it is:

$$k_{eff,def} = \frac{\mu W}{300\ mm} + W \cdot \frac{4 \cdot \pi^2}{g \cdot T^2} = \frac{777{,}8\ kN}{300\ mm} \cdot \left(0{,}04 + \frac{4 \cdot 3{,}14^2}{9810\ \frac{mm}{s^2} \cdot (4\ s)^2} \cdot 300\ mm \right)$$
$$= 0{,}299\ \frac{kN}{mm}$$

Also the effective stiffness obtained from the constitutive law reflects the one obtained with reference to the theoretical definition, unless of some negligible differences due to the approximation of the values assumed for the various parameters.

The numerical modelling is therefore correctly defined as the constitutive law in Figure 16 reflects the theoretical response of the isolators. To characterize an isolator, it is then necessary to identify optimal values for the friction factor and the horizontal stiffness.

As a starting hypothesis, it was assumed to have isolators of equal stiffness, assuming different values of the period of the isolation system and of the friction factor. The three most significant cases of this initial phase are reported in Table 3, in which the results in terms of displacement of the isolators have been obtained from the analyses carried out adopting the high seismic intensity accelerogram ED74.

Case	Modelling assumptions			Max displacements	
	Friction [%]	T_{is} [s]	k [kN/mm]	$\lvert s_{x,max} \rvert$ [cm]	$\lvert s_{y,max} \rvert$ [cm]
1	3	4	0,187	22,8	27,3
2	4	3	0,332	22	20,6
3	4	2,5	0,478	17,9	16,7

Table 3 First iterative phases

In general it can be observed that, by increasing the stiffness of the isolators and thus decreasing their period, the maximum displacements of the isolators in the two directions decrease.

One disadvantage when allowing high displacements in the devices is that this might easily result in increments of the displacements incompatible with the maximum allowable dis-

placements of the isolators. This is the most dangerous condition since exceeding the limit displacement might cause failure of the isolators and furthermore a sudden stop of the structure with high impact forces, a sort of hammering at the base of the structure.

On the other hand, limiting the displacements has the primary disadvantage that in this way smaller displacements are allowed. The dissipated seismic energy will also be lower and therefore the isolation system may not be sufficient to completely protect the structure. High stress concentrations might occur, although locally, which might lead to plasticization or extreme loading conditions in the connections.

Even considering an isolation system with period equal to 4 seconds, plasticisation of columns occurs in the first floor, as shown in Figure 17. For the cases 2 and 3, the stresses in the structure increase even more and not negligible plasticization occurs also in the top of the columns.

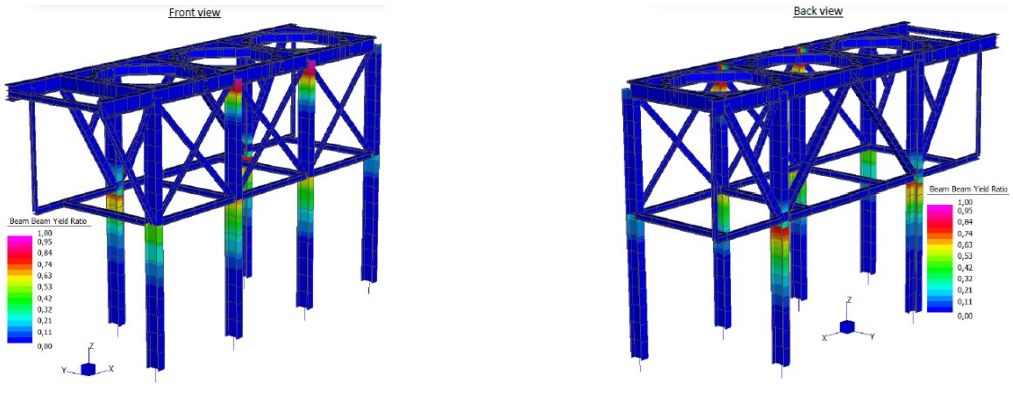

a. Case 1 – Side with X bracing

b. Case 1 – Side with chevron bracing

Figure 17 Inelastic behaviour observed with isolators placed at the column bases

This effect is due to additional torsional effects, caused by different displacement time histories experienced by the isolators, which cause rotations of the structure in the x - y plane (Figure 18).

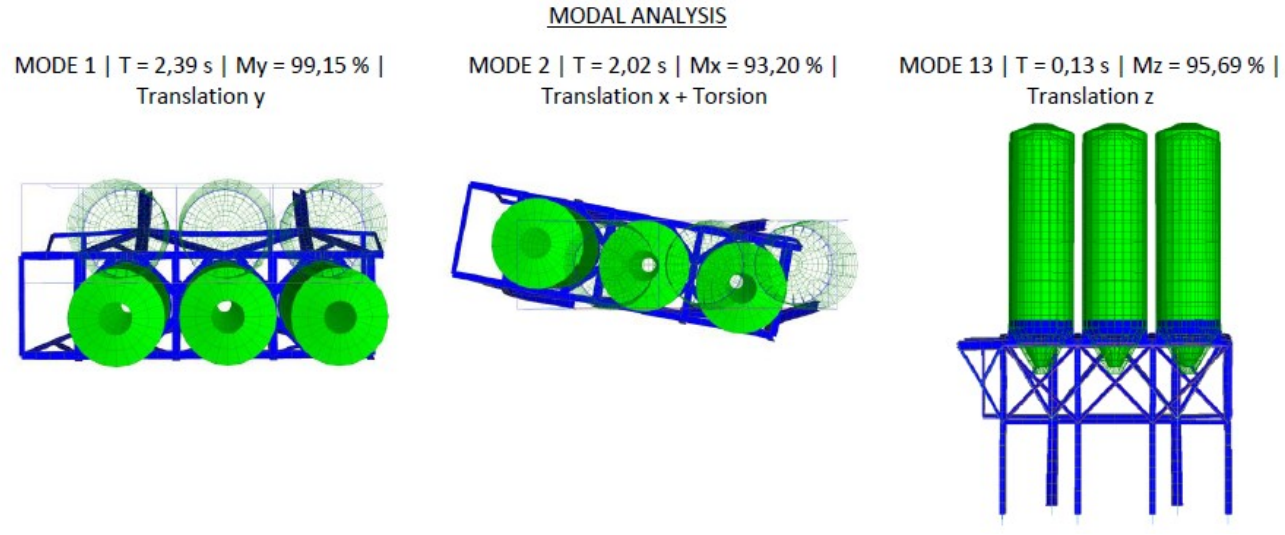

Figure 18 Torsional effects in the structure.

For example, in case 1 with isolators having a period of 4 seconds and a friction factor 3 %, it can be noticed that the isolator displacements in the x-direction (Figure 19) and in the y-direction (Figure 20) are not uniform, since the isolators are not connected with each other. Approximately after 12 seconds, the maximum difference between the displacement of the two isolators along x is approximately about 15 cm.

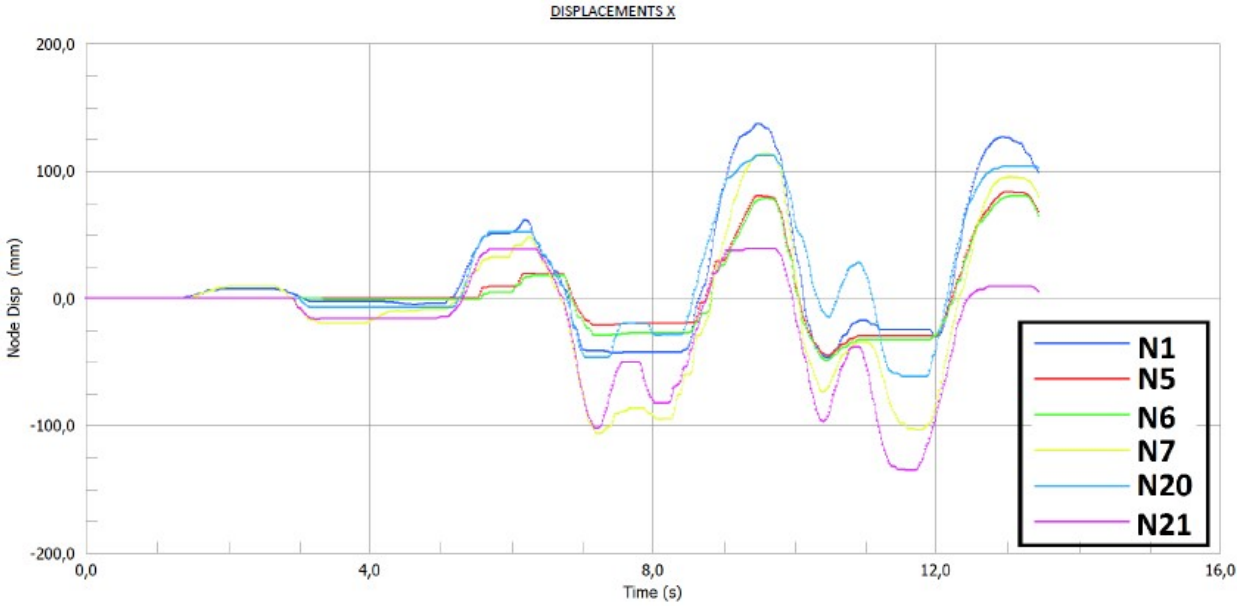

Figure 19 Isolator displacements along x-direction of the isolated structure for case 1

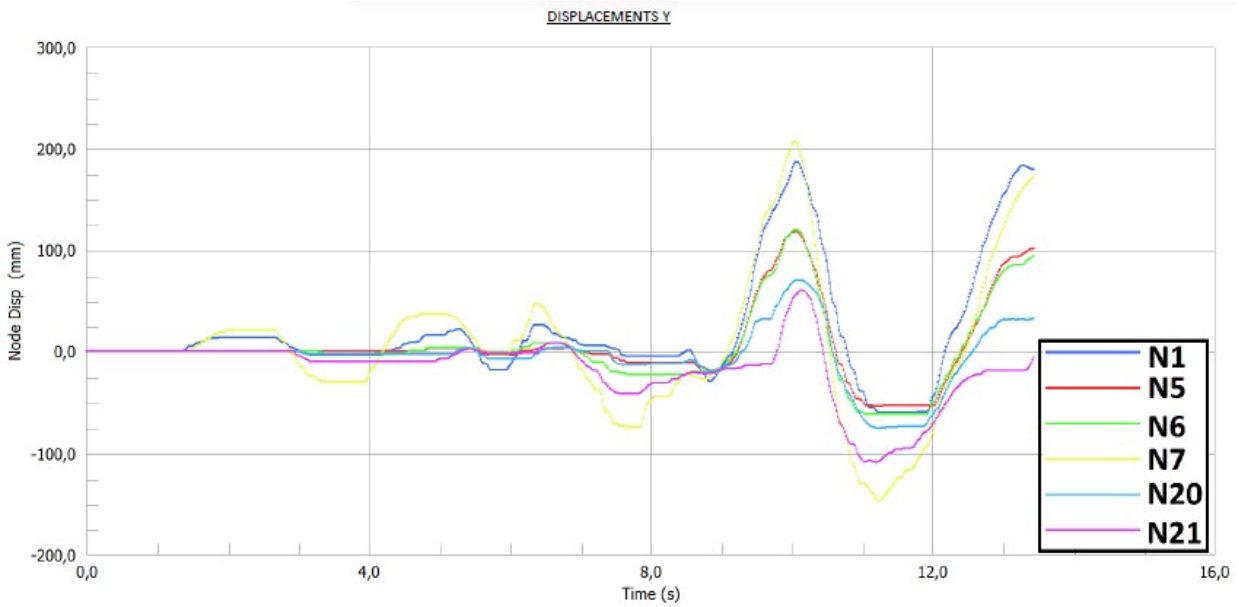

Figure 20 Isolator displacements along y-direction of the isolated structure for case 1

Such a solution is not optimal. To force the isolators to have the same displacement, and then get a translational motion in the x - y plane, different alternatives can be considered. Several solutions have been analysed to solve this asymmetry problem (Figure 21)

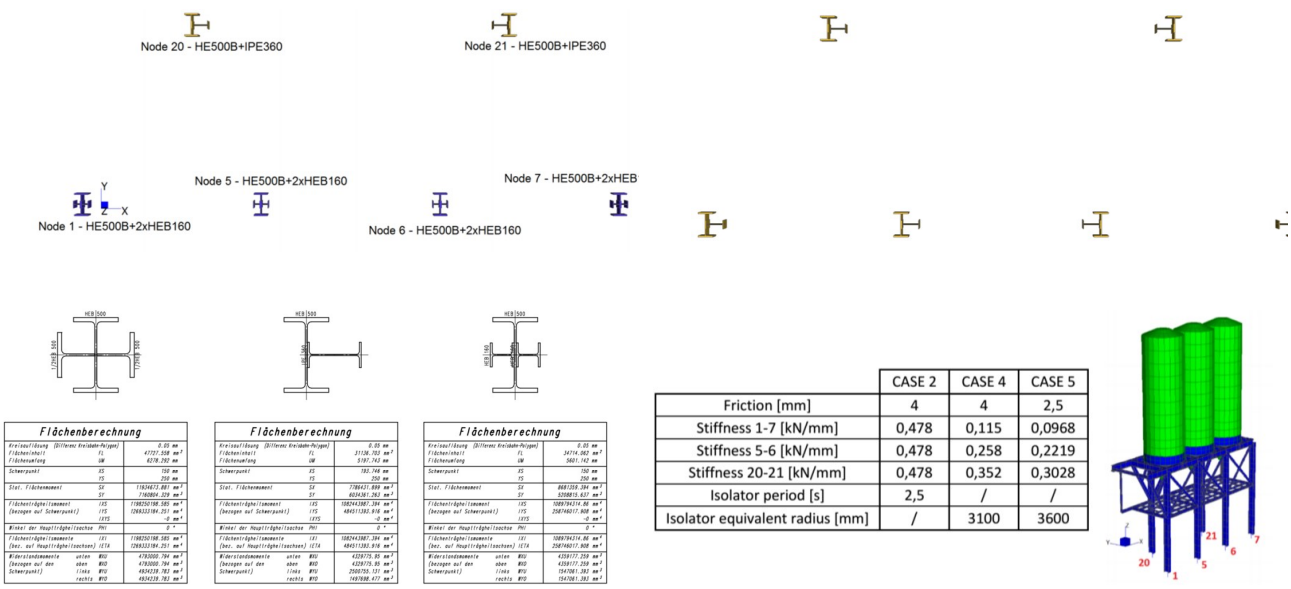

	CASE 2	CASE 4	CASE 5
Friction [mm]	4	4	2,5
Stiffness 1-7 [kN/mm]	0,478	0,115	0,0968
Stiffness 5-6 [kN/mm]	0,478	0,258	0,2219
Stiffness 20-21 [kN/mm]	0,478	0,352	0,3028
Isolator period [s]	2,5	/	/
Isolator equivalent radius [mm]	/	3100	3600

Figure 21 Different Retrofit strategies tried to solve asymmetry issue

After several iterations, the best solution has been obtained by using 6 seismic isolators connected by a rigid diaphragm made of as a horizontal steel frame with beams and horizontal bracing elements at ground level as shown in Figure 22. Solutions without a rigid diaphragm did not provide a feasible solution because of excessive global torsional behaviour.

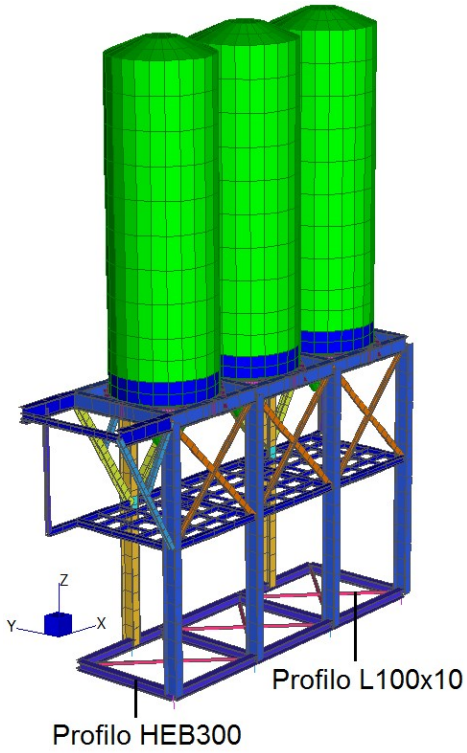

Figure 22 Retrofitted silo system

Horizontal stiffness and friction parameters have been iterated to find an optimal balance between best structural performance and acceptable maximum displacements. Inelastic deformations on the steel structure have been avoided (Figure 23).

Case	Modelling hypotheses					Max displacements	
	Friction coefficient [%]	T_{is} [s]	$k_{1,7}$ [kN/mm]	$k_{5,6}$ [kN/mm]	$k_{20,21}$ [kN/mm]	$\|s_{x,max}\|$ [cm]	$\|s_{y,max}\|$ [cm]
4	4	4	0,09	0,2	0,274	14,2	24,8
5	4	3,5	0,118	0,263	0,358	14,3	23,6
6	4	3	0,16	0,357	0,488	12,3	21,8
7	3	3	0,16	0,357	0,488	15,4	25,2
8	4	2,5	0,23	0,515	0,7	12,6	20,1
9	3	2,5	0,23	0,515	0,7	14,6	21,1

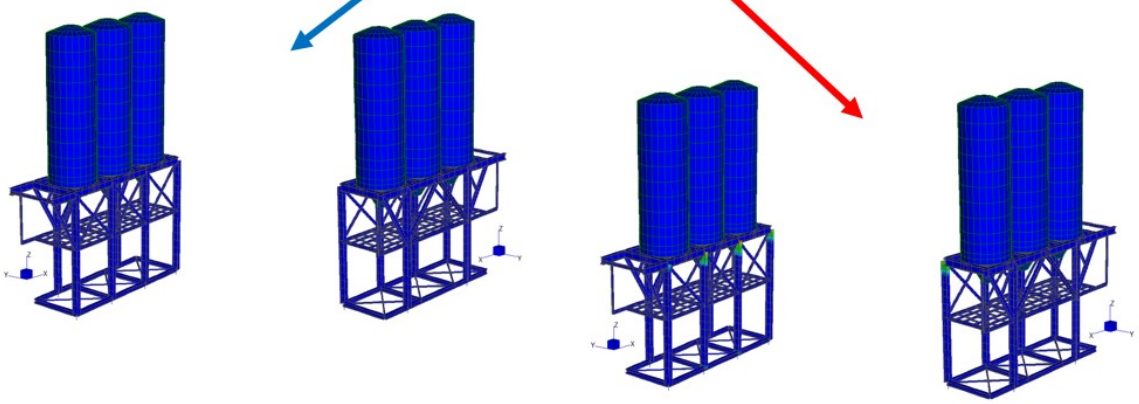

Figure 23 Comparison of retrofit solution 4 and 8: In case 4, full elastic behaviour can be obtained

Table 4 shows the most suitable isolator properties obtained after several iterations. Please note that different horizontal stiffness values have been used for different supports, which are calibrated according to the vertical reaction force under full-silo gravity loading condition.

Isolator properties	
Friction	4%
T_{is}	4 seconds
$k_{1,7}$	0,09 kN/mm
$k_{5,6}$	0,2 kN/mm
$k_{20,21}$	0,274 kN/mm
k_v	3000 kN/mm

a. Isolator properties

Nodo	F_z [kN]
1	358,3
5	777,8
6	798,8
7	340,2
20	1090,2
21	1080,7

b. Nodal reaction of structure supports

Table 4 Isolator properties and nodal reactions

Modal shapes and values are shown in Figure 24 and Table 5.

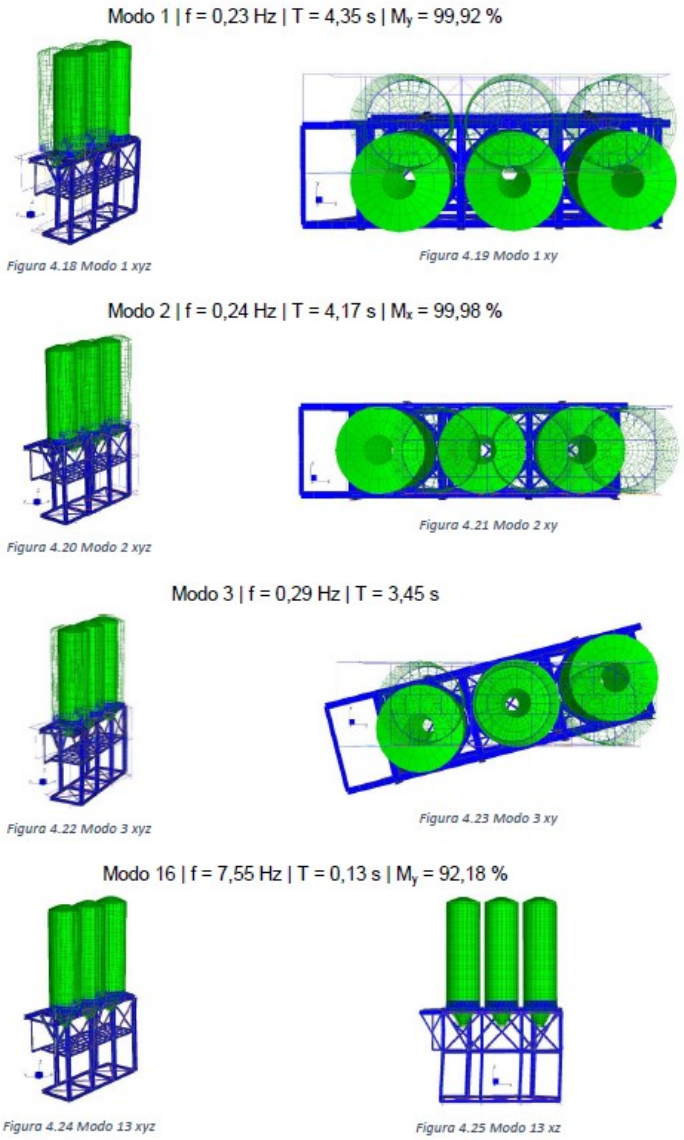

Figure 24 Modal shapes of retrofitted solution

Mod	T [s]	Direction
1	4,35	y (transversal)
2	4,17	x (longitudinal)
3	3,45	Torsional
16	0,13	z (vertical)

Table 5 Modal analysis results

To quantify the performance of the selected isolators, 7 nonlinear time history analysis have been performed. Max/min values of isolator displacements and residual displacements obtained from each accelerogram, and as an average of 7 accelerograms are shown in Table 6 and Figure 25.

Seismic Input	Max displacement of isolators [cm]		Max residual displacement of isolators [cm]	
	x	y	x	y
ED74	14,0	24,5	3,72	4,21
ED196	3,8	2,6	1,14	1,64
ED535	34,5	29,0	0,84	1,13
ED6349	5,6	29,0	1,43	1,45
IN113	21,2	11,9	3,23	2,21
IN331	29,3	41,2	1,58	2,31
IN461	21,3	33,9	0,79	2,06
Avg	**18,5**	**24,2**	**1,86**	**2,12**

Table 6 Max/Min displacements

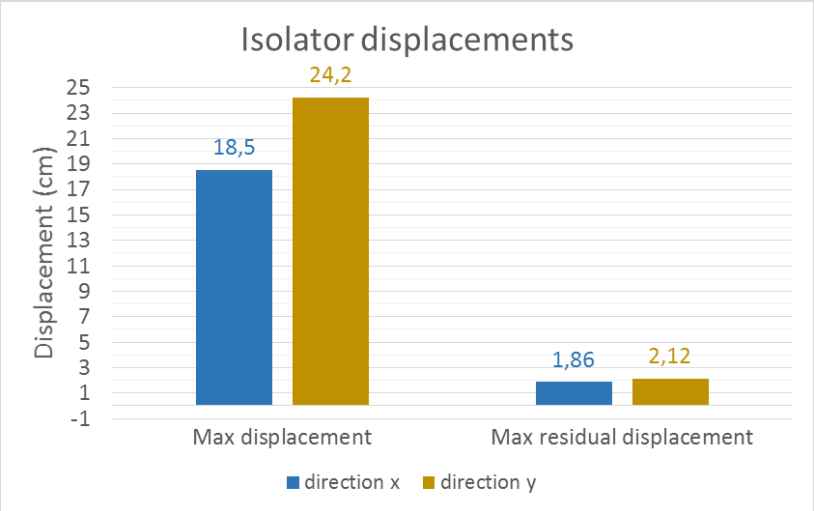

Figure 25 Max/Min displacements

Max/min values of base shear and relative displacements of the structure's mass center obtained from each accelegoram, and as an average of 7 accelerograms are shown in Table 7 and Figure 26.

Seismic Input	Base shear [kN]		Relative displacements of structure mass center [cm]	
	x	y	x	y
ED74	374,5	287,3	5,1	9,4
ED196	272,0	138,4	3,8	5,2
ED535	538,7	303,3	8,8	9,3
ED6349	165,1	419,0	2,2	11,1
IN113	487,1	167,4	7,1	5,8
IN331	607,8	513,3	11,6	17,4
IN461	480,1	448,2	7,4	14,4
Average	**417,9**	**325,3**	**6,6**	**10,4**

Table 7 Max/Min displacements and base shear

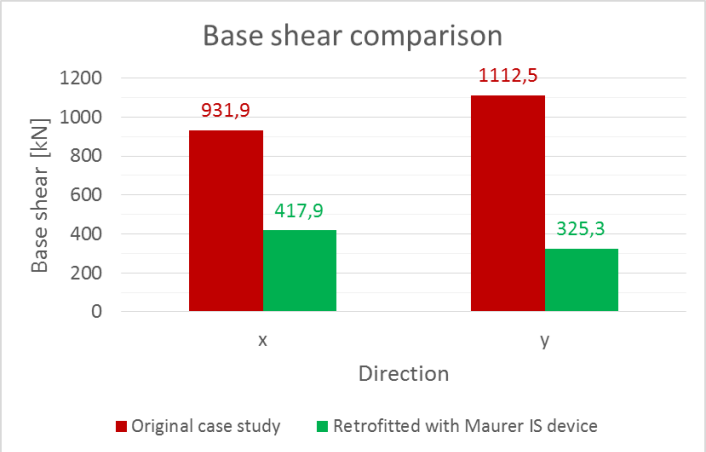

Figure 26 Max/Min base shear

Reductions in mean relative displacements of the two storeys are shown in Figure 27 for x and y directions.

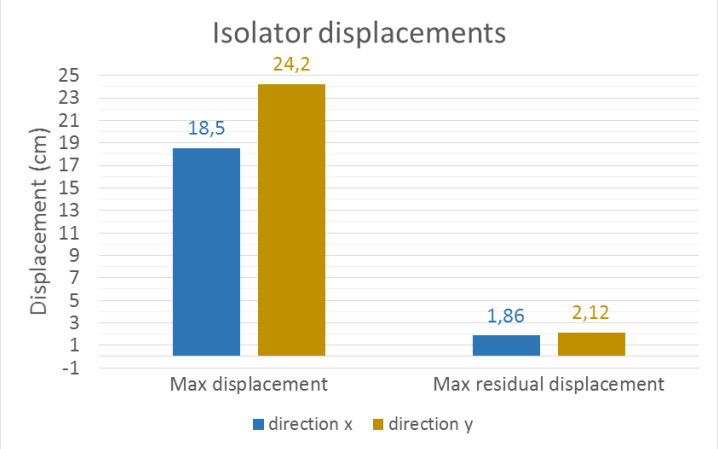

Figure 27 Reductions in mean relative displacements

Comparisons in terms of floor drifts are shown in Figure 28, Figure 29, and Table 8. The weak floor in the longitudinal direction of the structure is the first one, as the second floor is braced. The bracing was effective already in the case of a fixed base structure, wherein the average relative movement in the x direction of the second floor was equal to about 0.1%. In the isolated-base structure, the average relative movement of the second floor in the x direction is of 0.05% and is then maintained almost in the same order of magnitude as the previous case. In any case, the mean relative movement of the second plane in the direction x is negligible, and the reduction of 50% is relative and has just a minor impact on the structural response.

On the contrary, the first floor benefits from the isolation system. In particular in the x-direction (braced), in which the first floor is weak, the reduction is significant (approximately 64%) and the average relative displacement falls from a critical value equal to 3.49% in a fixed base structure to a value 1.24%.

In transverse y-direction (non-braced) a reduction of 35% for the first floor and 53% for the second floor can be observed. Also in this direction the structure takes advantage of the

isolation system, with limited mean relative displacements for both floors, unlike the fixed-base system in which values larger than 1.5% could be observed.

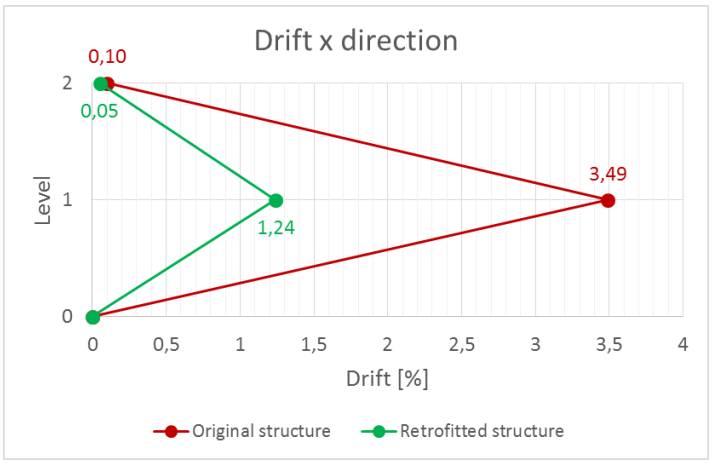

Figure 28 Drift comparison in x direction

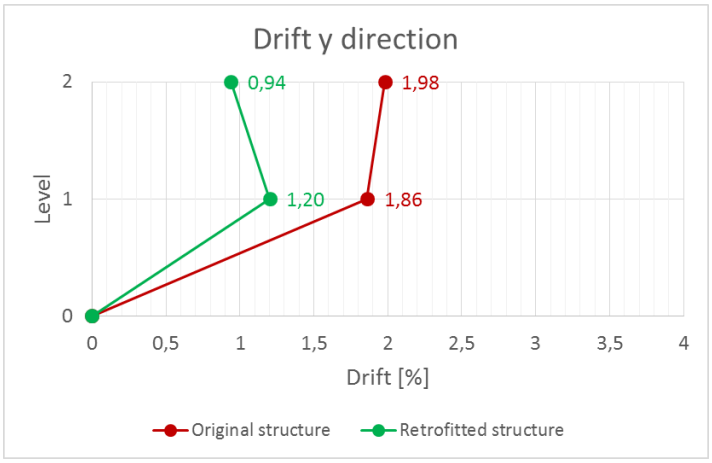

Figure 29 Drift comparison in y direction

Average interstorey drift				
Floor	Direction	Fixed-base structure	Isolated structure	Reduction
1	x	3,49 %	1,24 %	64 %
	y	1,86 %	1,20 %	35 %
2	x	0,10 %	0,05 %	50 %
	y	1,98 %	0,94 %	53 %

Table 8 Comparisons in terms of floor drifts

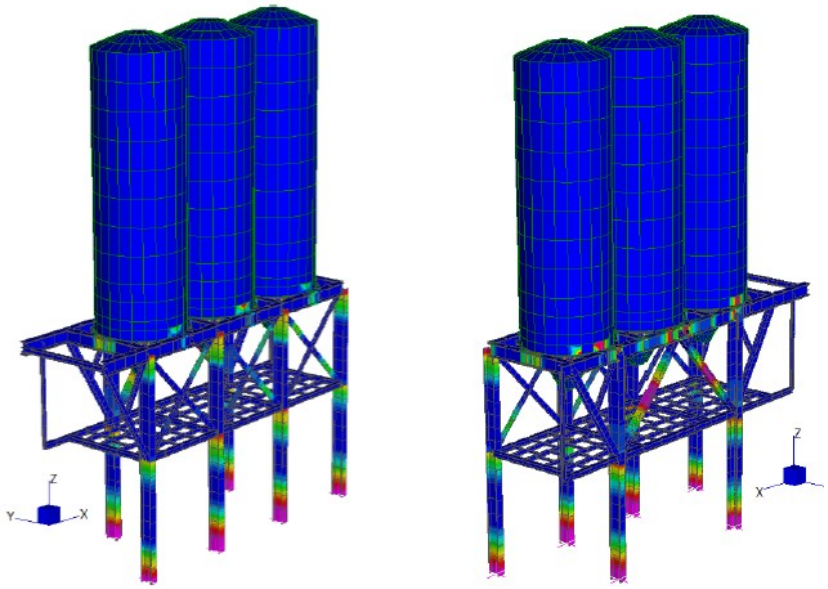

Figure 30 Yield index of the original structure

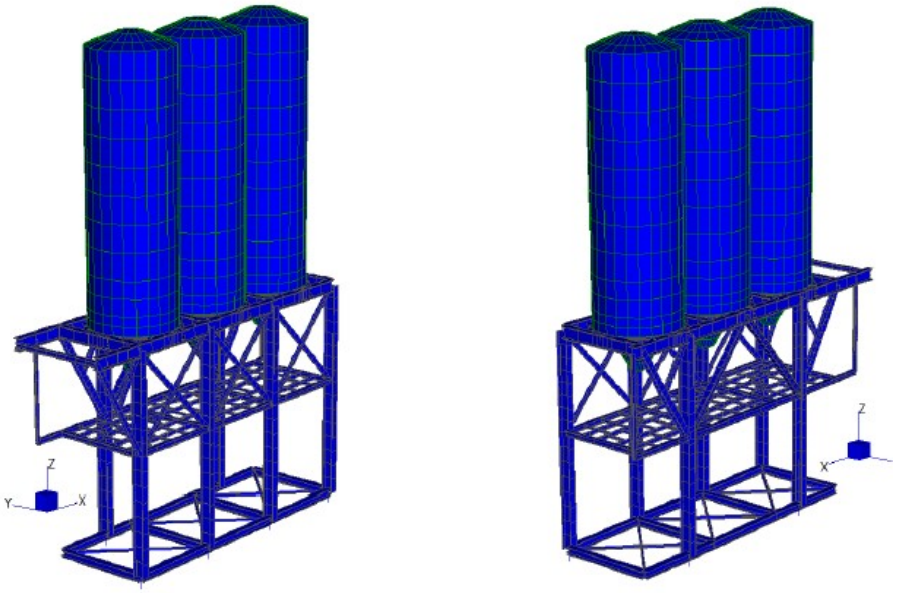

Figure 31 Yield index of the retrofitted structure

The yield index of the original and retrofitted structure can be compared from Figure 30 and Figure 31, with reference to the ED74 accelerogram. The retrofitted structure remains fully elastic.

5 IDA RESULTS IN HIGH SEISMICITY

Results of the IDA analysis based on high seismicity accelerograms are shown in terms of peak displacements and total base shear. For peak displacements, the control node is taken as the center of gravity of whole system. (x direction: longitudinal, y direction: transversal, z direction: vertical).

From Figure 32, it is seen that in general, retroffited structure responses in a linear manner to the increase in global base shear forces with increasing scale factors, while a global elasto-plastic behaviour is evident in case of the original structure.

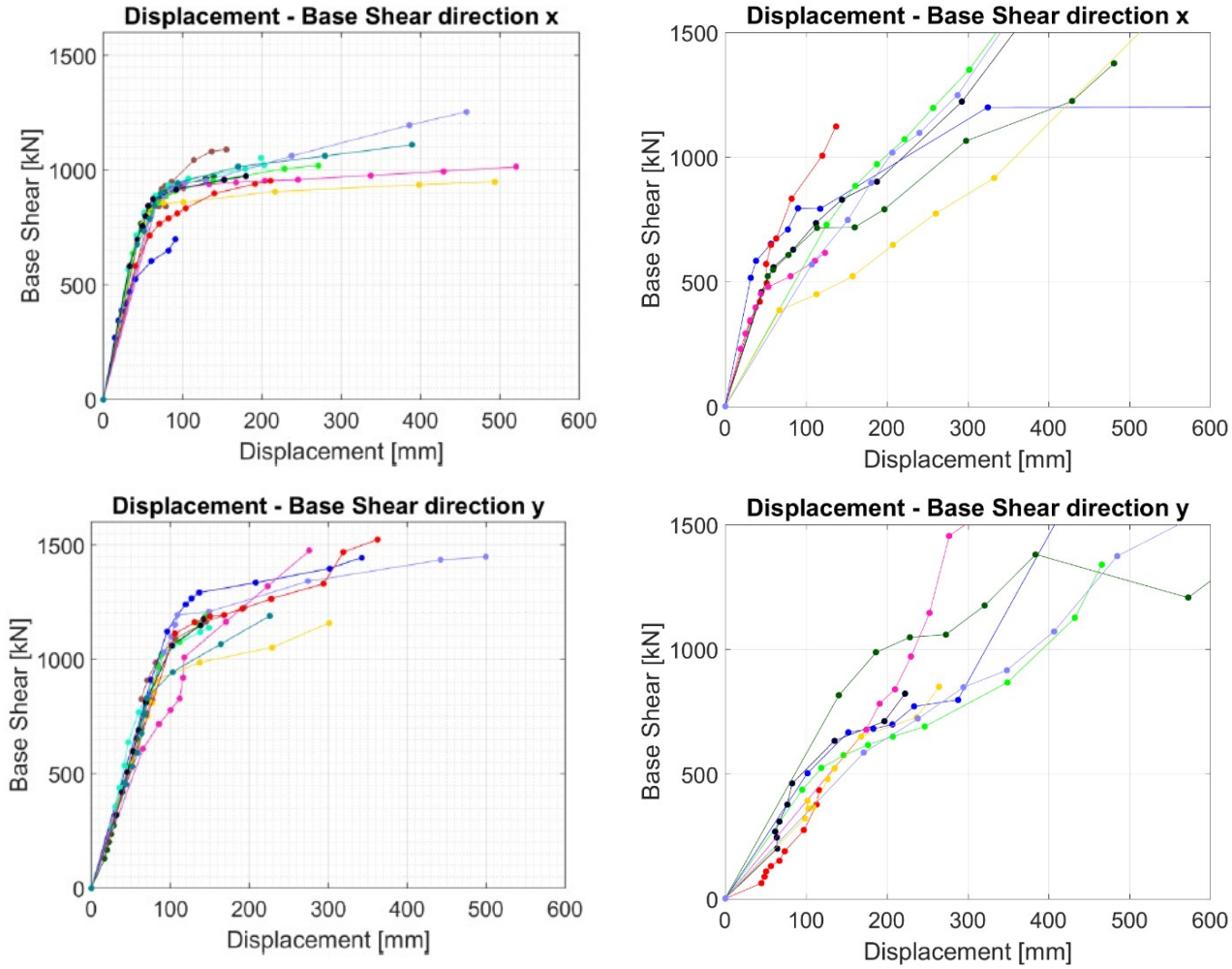

a. Original Structure b. Retrofitted structure

Figure 32 IDA results in terms of global displacement vs base shear

Figure 33 shows and Figure 34 show that drifts of both floors have been decreased significantly in case of retrofitted structure. Most importantly, the soft-storey behavior observed in the original structure has been eliminated thanks to the seismic retrofitting, as can be observed from the very low drift ratios of floor 1.

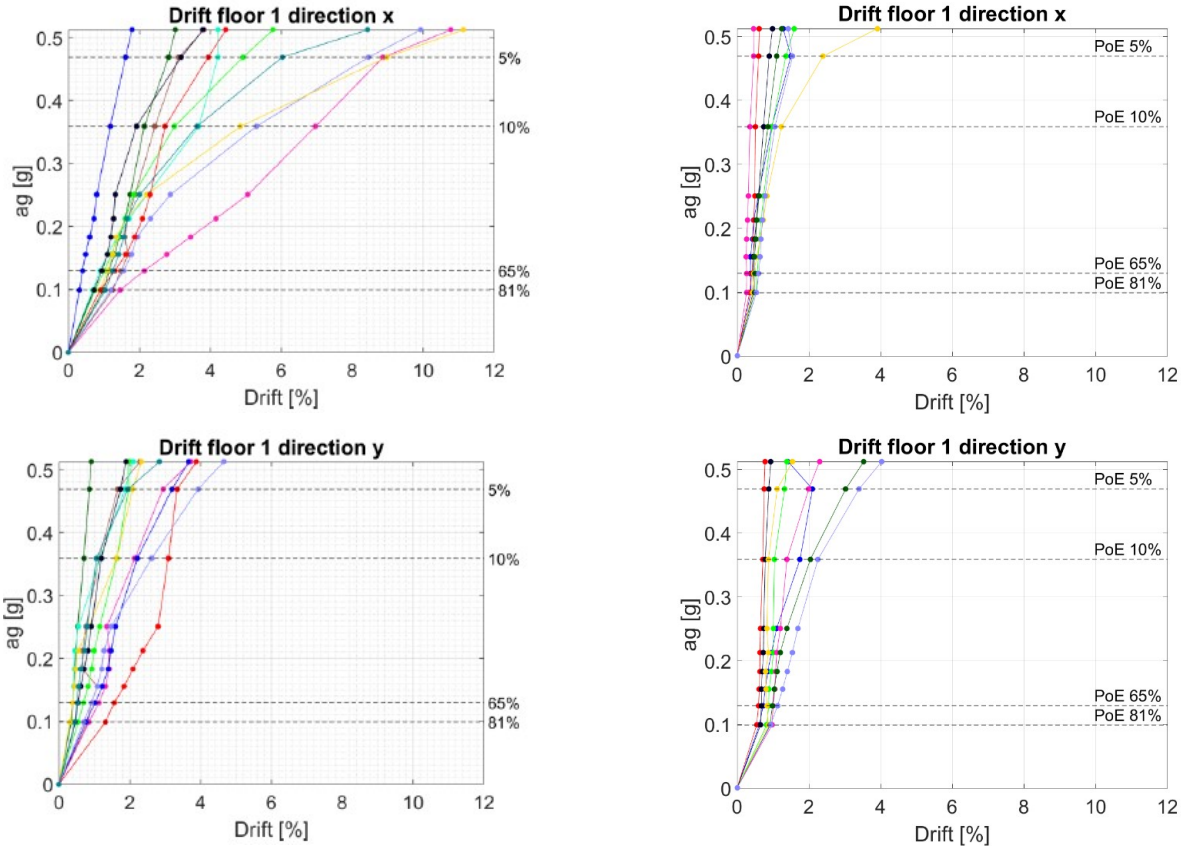

a. Original Structure b. Retrofitted structure

Figure 33 IDA results in terms of drift 1st floor

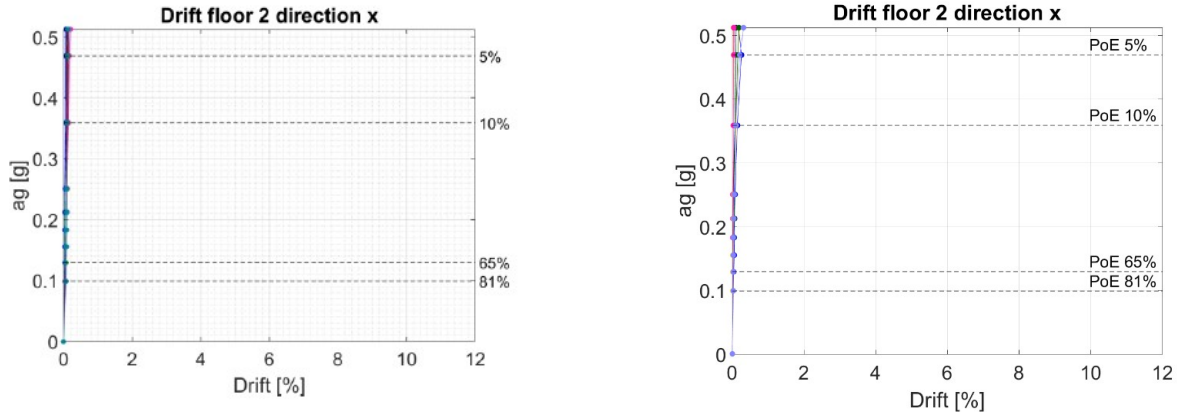

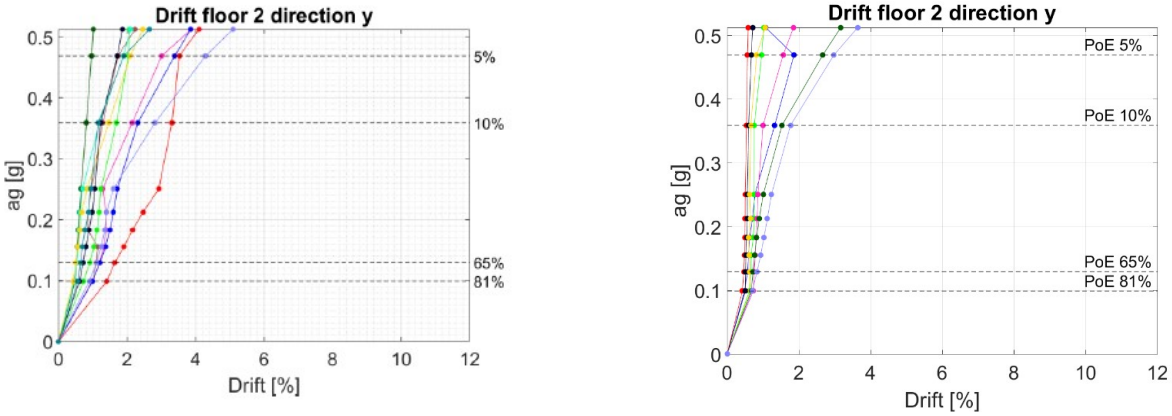

a. Original Structure

b. Retrofitted structure

Figure 34 IDA results in terms of drift 2nd floor

Although the global behavior of the structure is very satisfactory, in some cases, especially with high vertical earthquake component, uplift occurs (Figure 35). It could be avoided either with the introduction of proper ropes that prevent the uplifting of the isolation devices.

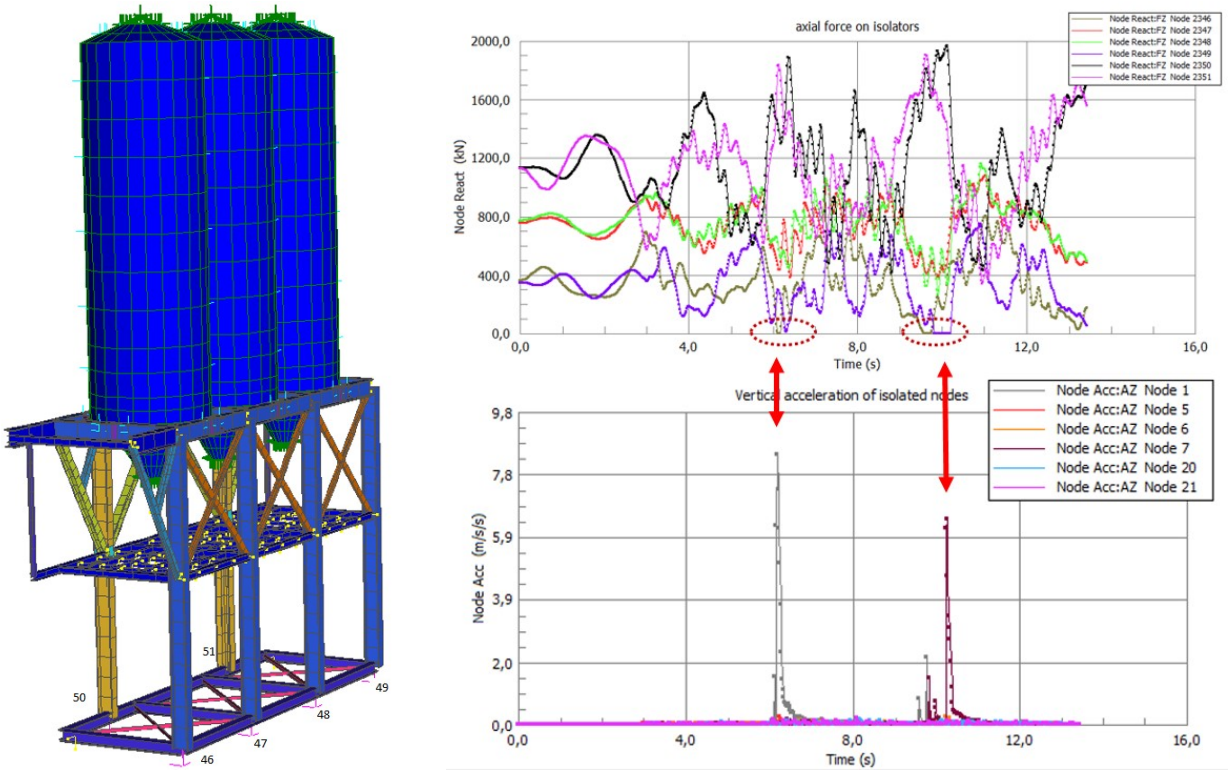

a. Retrofitted structure

b. Uplift instants during ED74 time-history (without vertical accelerations)

Figure 35 Uplift problem

In the cases with high vertical acceleration content (Figure 36), uplift is inevitable with the seismic isolation solution.

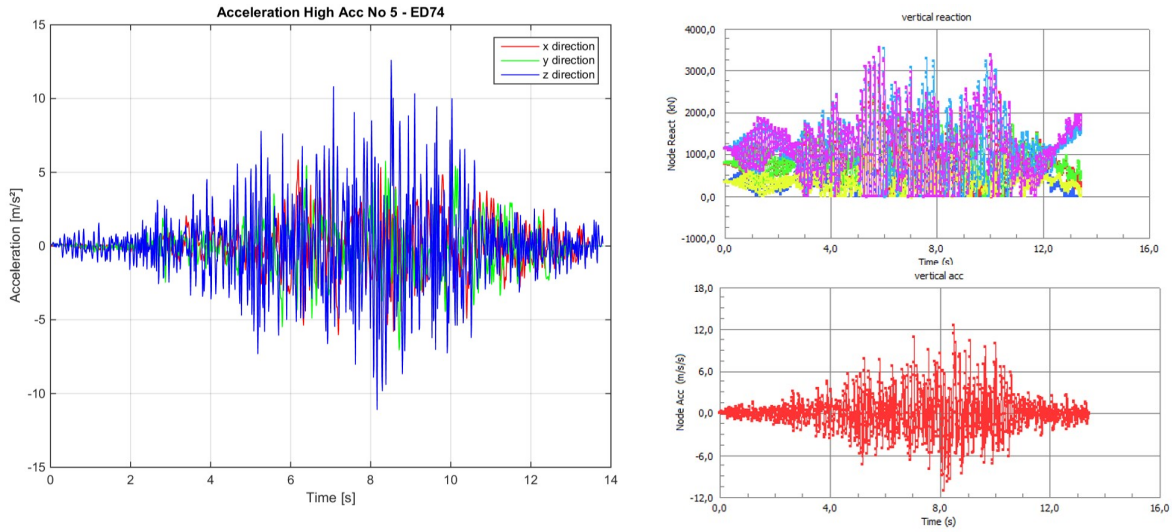

a. Three components of the ED74 time-acceleration history

b. Uplift instants during ED74 time-history (with vertical accelerations)

Figure 36 Uplift problem

To reduce the rocking effect and overturning moments which are the main causes of uplift, 2 other retrofitting strategies have been analysed:

i. Seismic isolators placed at the second floor level, under the silos

ii. Seismic isolators placed at the first floor level

The first approach resulted in global collapse of the system, causing high stresses in the beams which caused also a column loss and eventually the global collapse occurred (Figure 37). With the second approach, column bases suffer yielding due to second order effects caused by large displacements of isolated silos (Figure 38). Further analysis to investigate the performance of the structure with second retrofitting strategy is underway.

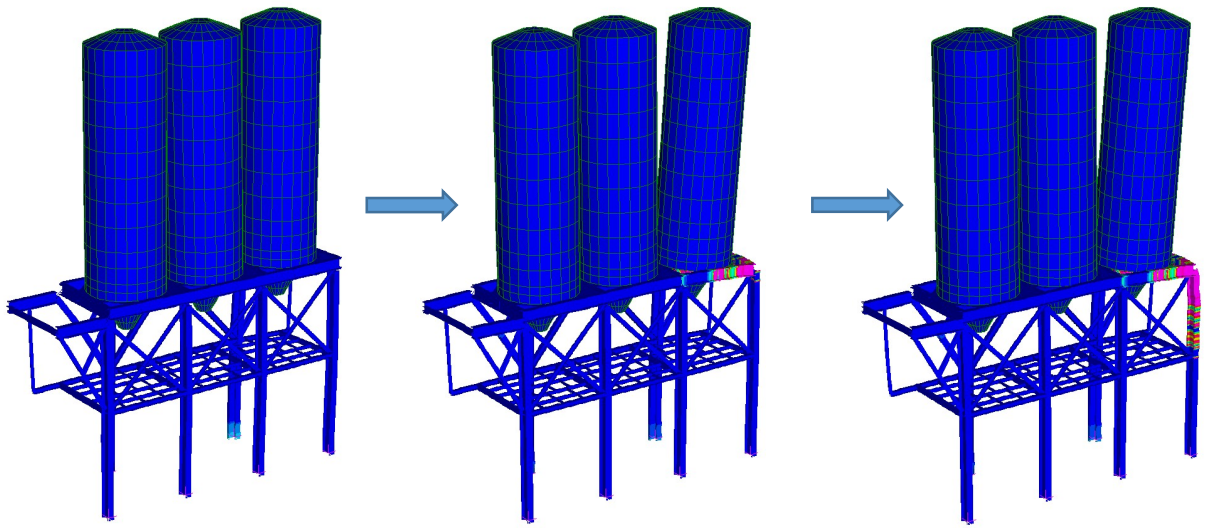

t= 6 sec t=8 sec (beam yielding starts) t=11 sec (column collapse)

Figure 37 Isolators placed at the second floor level, under the silos

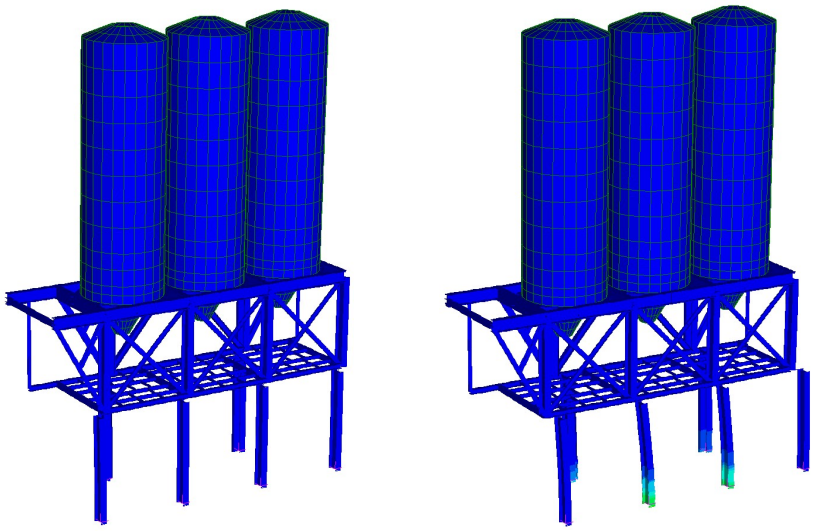

Figure 38 Isolators placed at the first floor level

It has also been noted that, vertical component of the earthquakes impact significantly the global behavior of the retrofitted structure. This can be seen from Figure 39, Figure 40, and Figure 41 where the red colored curves represents the global behavior with vertical component of the ED74 earthquake. When they are compared with the blue curves representing the global behavior without considering the vertical acceleration component, it is seen that achievement of the full elastic behavior will not be possible. In these cases, retrofitted solution can be seen as an improvement rather than a total rehabilitation solution.

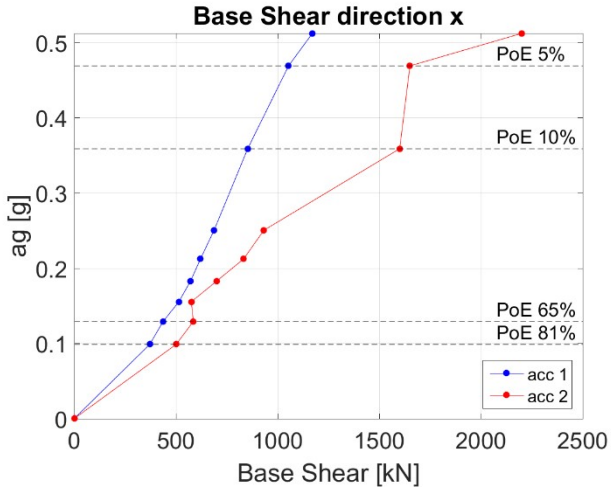

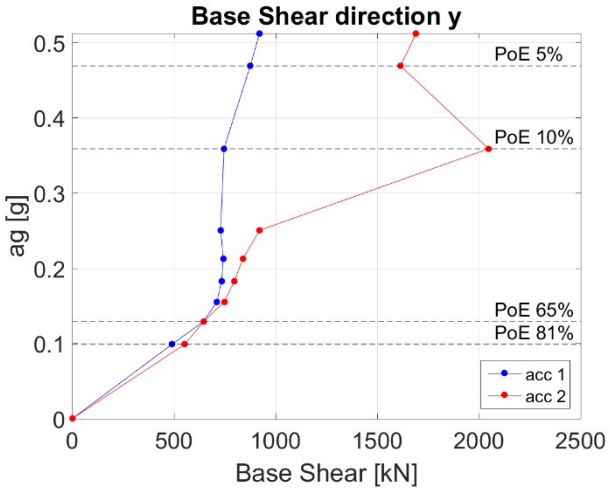

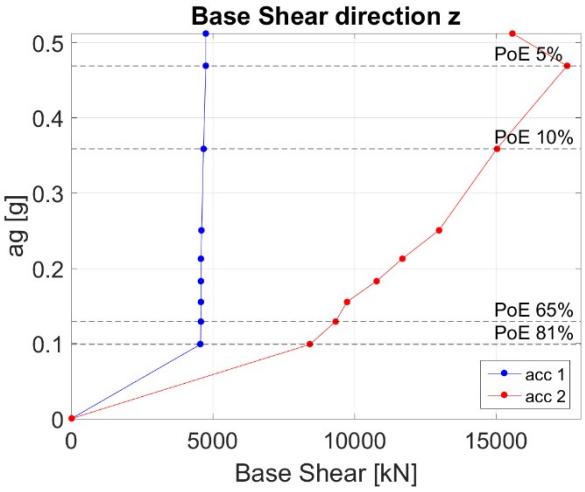

Figure 39 Impact of vertical component of ED74 earthquake in terms of base shear

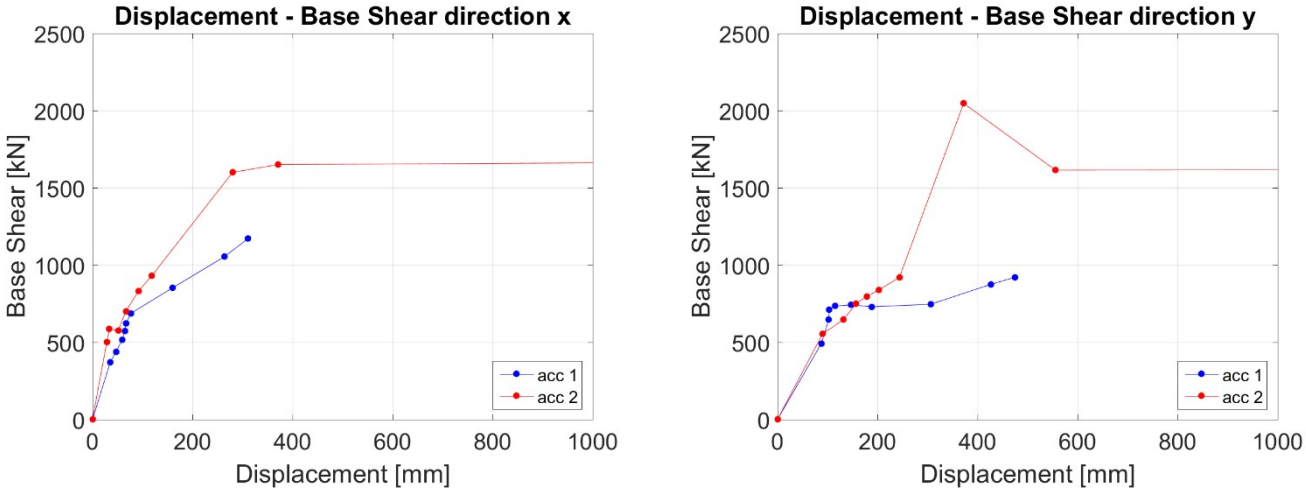

Figure 40 Impact of vertical component of ED74 earthquake in terms of displacement-base shear

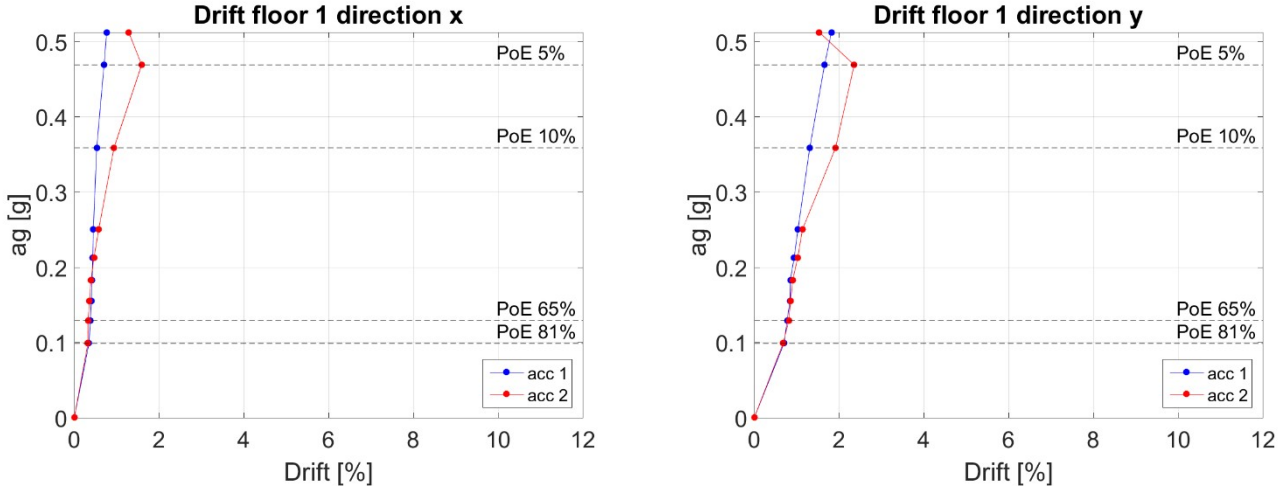

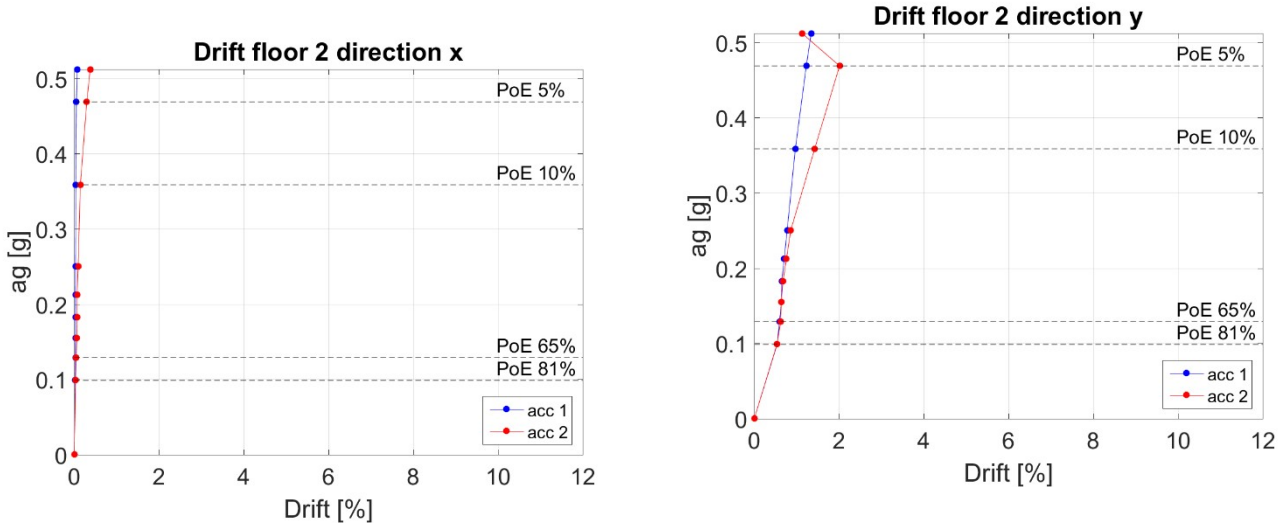

Figure 41 Impact of vertical component of ED74 earthquake in terms of floor drifts

6 CONCLUSIONS

The best seismic retrofit solution has been obtained by using 6 seismic isolators connected by a rigid diaphragm realized as a horizontal steel frame composed of beam and horizontal bracing elements at ground level. Global base shear values have been reduced significantly. Residual displacements of the retrofitted structure are very small, and much smaller than the residual displacements of the original structure. With the seismic retrofit, floor drifts are reduced, and the soft-storey behavior observed in the original structure has been eliminated. Vertical component of the earthquakes impact significantly the global behavior of the retrofitted structure. A fully elastic superstructure behaviour can be achieved only when the vertical component of earthquake is not significant. In summary, this retrofit solution improves significantly the seismic behaviour of the elevated silo system. In the final design of the isolators, uplift issue should be addressed.

REFERENCES

[1] 2nd Annual Report, EU-RFCS project PROINDUSTRY RFSR-CT-2013-00019

[2] A. Kanyilmaz, Inelastic Cyclic numerical analysis of steel struts using distributed plasticity approach, *COMPDYN 2015, 5th ECCOMAS Thematic Conference on Computational Methods in Structural Dynamics and Earthquake Engineering, Crete Island, Greece, 2015*

[3] E. Uckan, B. Akbas, J. Shen, R. Wen, K. Turandar, M. Erdik, Seismic performance of elevated steel silos during Van earthquake, October 23, 2011, *Natural Hazards*, January 2015, Volume 75, Issue 1, pp 265-287

[4] «MAURER Seismic Isolation with Sliding Isolation Devices for Bridge Structures,» Maurer Sohne, 2012.